

Cite this: *RSC Adv.*, 2014, 4, 65195

# Thermal stability, swelling behavior and CO<sub>2</sub> absorption properties of Nanoscale Ionic Materials (NIMs)<sup>†</sup>

Kun-Yi Andrew Lin,<sup>ab</sup> Youngjune Park,<sup>ac</sup> Camille Petit<sup>ad</sup> and Ah-Hyung Alissa Park<sup>\*a</sup>

Nanoscale Ionic Materials (NIMs) consist of a nanoscale core, a corona of charged brushes tethered on the surface of the core, and a canopy of the oppositely charged species linked to the corona. Unlike conventional polymeric nanocomposites, NIMs can display liquid-like behavior in the absence of solvents, have a negligible vapor pressure and exhibit unique solvation properties. These features enable NIMs to be a promising CO<sub>2</sub> capture material. To optimize NIMs for CO<sub>2</sub> capture, their structure–property relationships were examined by investigating the roles of the canopy and the core in their thermal stability, and thermally- and CO<sub>2</sub>-induced swelling behaviors. NIMs with different canopy sizes and core fractions were synthesized and their thermal stability as well as thermally- and CO<sub>2</sub>-induced swelling behaviors were determined using thermogravimetry, and ATR FT-IR and Raman spectroscopies. It was found that the ionic bonds between the canopy and the corona, as well as covalent bonds between the corona and the core significantly improved the thermal stability compared to pure polymer and polymer/nanofiller mixtures. A smaller canopy size and a larger core fraction led to a greater enhancement in thermal stability. This thermal stability enhancement was responsible for the long-term thermal stability of NIMs over 100 temperature swing cycles. Owing to their ordered structure, NIMs swelled less when heated or when they adsorbed CO<sub>2</sub> compared to their corresponding polymers.

Received 18th September 2014

Accepted 7th November 2014

DOI: 10.1039/c4ra10722e

www.rsc.org/advances

## 1. Introduction

Nanoscale Ionic Materials (NIMs), a new class of polymer grafted “hairy” nanoparticles, consist of a nanoscale core, a corona of charged brushes tethered on the surface of the core, and a polymeric canopy of oppositely charged species linked to the corona. Unlike conventional surface-modified nanostructures (e.g., polymeric nanocomposites)<sup>1–3</sup> and functionalized nanoparticles<sup>4,5</sup> which were usually solid,<sup>6–11</sup> some NIMs displayed liquid-like behaviors in the absence of solvents.<sup>12,13</sup> Since in liquid-like NIMs, the canopy species were found to strongly interact with the corona, they were strongly linked to the core and exhibited negligible vapor pressure.<sup>14–20</sup> The electrostatic

repulsion between the cores of NIMs<sup>21</sup> together with the incompressibility nature of NIMs<sup>22</sup> forced the polymer chains of the canopy to stretch out radially. This unique conformation conferred NIMs an unusual solvation property driven by entropy.<sup>16,20</sup>

Considering their negligible vapor pressure and unique solvation property, NIMs could be used as absorbents. Recently, NIMs were tested for CO<sub>2</sub> and promising CO<sub>2</sub> loading, recyclability and selectivity towards CO<sub>2</sub> were reported.<sup>14</sup> It was found that adsorption in NIMs was driven by their unique conformation which created some free space where CO<sub>2</sub> could be physically retained.<sup>16</sup> In addition to this entropic effect, chemical interactions also played a role when the polymer chains in NIMs were functionalized with task-specific groups.

Previous studies highlighted some aspects of the structure–property relationships of NIMs and showed that the canopy conformation could be skillfully tuned to enhance CO<sub>2</sub> capture. Beyond capture capacity, other properties relevant to carbon mitigation may be modulated by changing the structural features of NIMs. For instance, some research groups examined the role of the core in the properties of NIMs using different nanomaterials.<sup>21,23,24</sup> The canopy was also an important structural parameter since it accounted for about 60 to 80% of NIMs volume.<sup>25</sup> Considering this aspect, the present study aimed to investigate the roles of the canopy and core on specific NIMs

<sup>a</sup>Departments of Earth and Environmental Engineering & Chemical Engineering, Lenfest Center for Sustainable Energy, Columbia University, New York, NY 10027, USA. E-mail: ap2622@columbia.edu; Fax: +1-212-854-7081; Tel: +1-212-854-8989

<sup>b</sup>Department of Environmental Engineering, National Chung Hsing University, 402 Taiwan, Republic of China

<sup>c</sup>SK Innovation, 325, Exporo, Yuseong-gu, Daejeon 305-712, Republic of Korea

<sup>d</sup>Department of Chemical Engineering, Imperial College, London, SW7 2AZ, UK

<sup>†</sup> Electronic supplementary information (ESI) available: General synthesis procedures for preparing NIMs; schematics of the ATR FT-IR spectroscopy set-up; TGA results of PEGs, ionized PEGs and NIMs; TGA result of NIMs with the same core fraction but different canopy sizes; CO<sub>2</sub> solubility of NIMs as a function of CO<sub>2</sub> partial pressure; Raman spectra in the  $\nu_{\text{as}}(\text{CH}_2)$  and  $\nu_{\text{s}}(\text{CH}_2)$  regions for PEGs and NIMs. See DOI: 10.1039/c4ra10722e

properties that were relevant to CO<sub>2</sub> capture namely, the thermal stability and the swelling behaviors.

The thermal stability was studied as it impacts the ability of the capture materials to withstand the mild to high temperatures of the cyclic adsorption/regeneration process of CO<sub>2</sub> capture.<sup>14,15</sup> In addition, the temperature and/or the adsorption of molecules could modify the conformation of the polymer chains in the canopy, thereby causing changes in the bulk properties of NIMs such as the swelling. The measurement of swelling could therefore be used as a tool to study how NIMs responded to heating and to the adsorption of CO<sub>2</sub> molecules. Finally, varying the canopy size was expected to change the response of NIMs to these environmental changes (*i.e.*, thermal stability and swelling).

In this study, three NIMs with different canopy sizes were synthesized using polyethylene glycols (PEGs) with molecular weights (MW) of 1000, 2000, and 5000 Da. Thermal stabilities of these three NIMs were tested to investigate the effect of the canopy size. To isolate the role of the canopy, the thermal stabilities of NIMs were compared to those of three modified PEGs. To study the role of the core, a series of NIMs with a fixed core fraction as well as a mixture of PEG and cores were synthesized and their thermal stabilities were tested. In addition, we examined the effect of the canopy size on NIMs' thermally-induced and CO<sub>2</sub>-induced swellings using Attenuated Total Reflectance (ATR) Fourier-transform infrared (FT-IR) spectroscopy. These swelling behaviors reflected the conformational changes of the polymeric canopy caused by elevated temperatures or the presence of CO<sub>2</sub> molecules. These conformational changes were assessed by Raman spectroscopy.

## 2. Experimental section

### 2.1. Synthesis of NIMs and the corresponding ionized polymers

NIMs samples were synthesized according to the reported procedure<sup>14</sup> as shown in Fig. 1 and the general synthesis procedures can be found in the ESI.† To synthesize NIMs with different canopy size, amine-terminated polyethylene glycol polymers with MW of 1000, 2000 or 5000 (Richman Chemical USA) were used to form the canopy. 3-(Trihydroxysilyl)-1-propane sulfonic acid (THOPS) (Gelest USA) was selected to silanize the silica nanoparticles (Ludox HS-30, Sigma-Aldrich USA) and form the corona. Depending on the desired core fraction of the NIMs sample, the addition of the polymer was conducted either up to the equivalence point or up to a desired polymer/silica ratio. In this study, the synthesized NIMs were denoted as NIM-PEG-MW-[wt% of nanoparticles], where "I" refers to the ionic bonding between THOPS and PEG, "MW"

were 1000, 2000 or 5000, and the "wt% of nanoparticles" were 5, 19 or 25 wt%. The NIMs synthesized *via* the addition of the polymer up to the equivalence point were labeled as NIM-PEG-MW-E, where "E" indicated the equivalence point.

Next, in order to mimic the tethered polymers in NIMs, ionized PEG samples were prepared *via* an acid-base reaction between the amine-terminated PEGs and silane. Briefly, the amine-terminated PEG and silane were diluted with deionized water into 10 wt% solutions. The silane solution was dropwise added to the PEG solution while monitoring the pH. Equivalence point plots were employed to ensure the 1 : 1 ratio of sulfonate groups (from silane) to amine groups (from PEGs). Finally, water was removed under vacuum at 35 °C. The derived materials were denoted as Ionized PEG1K, Ionized PEG2K and Ionized PEG5K, depending on the molecular weight of the polymer.

Finally, a physical mixture of 12 nm silica nanoparticles (LUDOX, Sigma-Aldrich) and PEG1K was prepared by simply mixing the aqueous suspension of silica nanoparticles with the polymer. The mixture was then dried at 35 °C under vacuum to remove the water. The derived sample was labeled as PEG1K/NP-25, where "NP" stood for nanoparticles and 25 referred to the weight percent of the nanoparticles in the mixture. The notations and compositions of all the prepared materials were summarized in Table 1.

### 2.2. Thermal stability and thermally-induced swelling behavior

Thermal stability experiments were conducted using a thermogravimetric analyzer (TA Instruments Q50, TGA). Each sample was heated from room temperature to 600 °C with a ramping rate of 5 °C min<sup>-1</sup> in an oxygen environment to identify its thermal decomposition temperature. In order to determine the long-term stability of NIMs under elevated temperatures, multi-thermal cycle tests were also performed by heating and cooling the sample cyclically from ambient temperature to a target temperature (*i.e.*, 100 cycles at 120 °C and 25 cycles at 140 °C) in an oxygen environment.

The thermally-induced swelling of NIMs was measured *via* ATR FT-IR spectroscopy using a Nicolet 6700 spectrometer (Thermo Fisher Scientific Inc.) equipped with an ATR cell consisting of a diamond crystal and a high-pressure cell (Golden Gate™ Supercritical Fluids Analyzer, Specac Ltd). The measurements were conducted from 60 to 120 °C which is a typical temperature range for CO<sub>2</sub> capture and release. A schematic diagram of the experimental set-up is shown in Fig. S1 (ESI†). In a typical test, a small amount of sample was deposited on the crystal surface, heated to the desired temperature and the spectrum was collected. All spectra were obtained from the

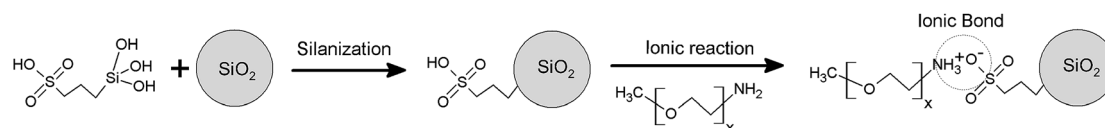







Fig. 1 Schematic of the synthesis of PEG-based NIMs.

Table 1 List of prepared NIMs and polymers

Category	Sample name	Description	Core fraction (wt%)
PEG  	PEG1K	Mono-amine terminated PEG of MW 1000	—
	PEG2K	Mono-amine terminated PEG of MW 2000	—
	PEG5K	Mono-amine terminated PEG of MW 5000	—
NIMs  	NIM-PEG1K-E	Chain = PEG <sup>a</sup> of MW 1000 at equivalent point <sup>b</sup>	25
	NIM-PEG2K-E	Chain = PEG of MW 2000 at equivalent point	19
	NIM-PEG5K-E	Chain = PEG of MW 5000 at equivalent point	5
	NIM-PEG2K-25	Chain = PEG of MW 2000 at 25 wt% core fraction	25
	NIM-PEG5K-25	Chain = PEG of MW 5000 at 25 wt% core fraction	25
Mixture of PEG and nanoparticles  	PEG1K/NP-25	Physical mixture of "PEG1K" and 25 wt% of silica nanoparticles	25
	Ionized PEG1K	Ionized "PEG1K" using THOPS <sup>c</sup>	—
	Ionized PEG2K	Ionized "PEG2K" using THOPS	—
Ionized PEG  	Ionized PEG5K	Ionized "PEG5K" using THOPS	—
	mPEG1K	Methoxy-PEG of MW 1000	—
	mPEG2K	Methoxy-PEG of MW 2000	—
mPEG  	mPEG5K	Methoxy-PEG of MW 5000	—

<sup>a</sup> PEG: polyethylene Glycol. <sup>b</sup> Anionic polymer chains : cationic sites on nanoparticles = 1 : 1. <sup>c</sup> THOPS: 3-(trihydroxysilyl)-1-propane sulfonic acid.

acquisition of 16 scans with a resolution of  $4\text{ cm}^{-1}$  and a spectrum range of  $4000\text{--}525\text{ cm}^{-1}$ . The thermally-induced swelling ( $S$ ) was then derived by monitoring the change in the  $\text{CH}_2$  stretching band of the polymeric canopy ( $\sim 2900\text{ cm}^{-1}$ ) using eqn (1) as described in prior studies:<sup>16,26,27</sup>

$$S = \frac{A^0}{A} \frac{d_e}{d_e^0} - 1 \quad (1)$$

where  $A^0$ ,  $d_e^0$ ,  $A$ , and  $d_e$  were the absorbance of the  $\text{CH}_2$  band and the effective path length at  $T_0$  ( $T_0 = 60\text{ }^\circ\text{C}$ ) and  $T$  ( $T = 70\text{ }^\circ\text{C}$  to  $120\text{ }^\circ\text{C}$ ), respectively. To simplify eqn (1), it was assumed that the effective path length was not significantly changed within the studied temperature range.<sup>16,26,27</sup>

### 2.3. $\text{CO}_2$ -induced swelling behavior

The  $\text{CO}_2$ -induced swelling behavior was determined using the same ATR FT-IR spectrophotometer equipped with a high-pressure cell set-up as for the temperature-induced swelling behavior. Chemical interaction between  $\text{CO}_2$  and NIMs were limited to van der Waals interactions since neither the corona nor the canopy had task-specific functional groups. Therefore the entropic contribution from the conformational changes could be probed. The ATR FT-IR setup could be used simultaneously to determine  $\text{CO}_2$ -induced swelling and  $\text{CO}_2$  capture capacity of NIMs. In a typical experiment, the sample was deposited on the surface of the ATR crystal, the high-pressure cell was closed and the temperature was set at  $60\text{ }^\circ\text{C}$ . Next,  $\text{CO}_2$  was injected into the chamber at a pressure ranging from

0.40 to 5.57 MPa. After reaching the equilibrium, the FT-IR spectra were collected 16 times with a resolution of  $4\text{ cm}^{-1}$ . The  $\text{CO}_2$ -induced swelling of NIMs was then calculated following the same approach as for the thermally-induced swelling calculation (eqn (1)). Note that in this case  $A^0$ ,  $d_e^0$ ,  $A$ , and  $d_e$  represented the absorbance of the  $\text{CO}_2$  stretching band and the effective path length without and with the exposure to  $\text{CO}_2$ , respectively.

The obtained FT-IR spectra could also be used to derive the  $\text{CO}_2$  capture capacity of the studied materials by employing the modified Beer-Lambert law. In ATR FT-IR spectroscopy, an effective thickness of the evanescent wave ( $d_e$ ), rather than actual path length was considered<sup>43</sup> for the Beer-Lambert law (eqn (2)):

$$A = \varepsilon C_{\text{CO}_2} d_e \quad (2)$$

where  $A$  was the absorbance,  $\varepsilon$  was the absorptivity (in  $\text{cm}^2\text{ mol}^{-1}$ ),  $C_{\text{CO}_2}$  was the concentration of  $\text{CO}_2$  in the sample (in  $\text{g-CO}_2$  per  $\text{cm}^3$ ), and  $d_e$  was the arithmetical mean between the effective path length for the perpendicular ( $d_{e\perp}$ ) and parallel ( $d_{e\parallel}$ ) polarization (in cm). For the calculation of  $d_e$ , the refractive indices of NIMs were required, which were measured by a refractometer (J357, Rudolph Research Analytical). The  $\text{CO}_2$  absorption capacity was then quantified by measuring the intensity of the  $\text{CO}_2$  asymmetric stretching band ( $\sim 2340\text{ cm}^{-1}$ ) and assuming its molar absorptivity at high-pressure as  $1.0 \times 10^6\text{ cm}^2\text{ mol}^{-1}$ . Finally, eqn (3) was used to determine the  $\text{CO}_2$  absorption capacity (in  $\text{mmol}_{\text{CO}_2}$  per g-solvent):<sup>15,41,42</sup>

$$\text{CO}_2 \text{ absorption capacity} = \frac{C_{\text{CO}_2}}{\text{MW}_{\text{CO}_2} y_p \frac{\rho_{\text{NIMs}}}{1+S}} \times 1000 \quad (3)$$

where  $\text{MW}_{\text{CO}_2}$  ( $\text{g mol}^{-1}$ ) was the molecular weight of  $\text{CO}_2$ ,  $\rho_{\text{NIMs}}$  was the density of the material,  $y_p$  was the polymer weight fraction and  $S$  was the  $\text{CO}_2$ -induced swelling.

#### 2.4. Raman spectroscopy

For the conformational investigation of NIMs, Raman spectra were collected at room temperature using a LabRAM ARAMIS spectrometer (Horiba Jobin Yvon) equipped with a microscope and a  $50\times$  objective. A solid-state frequency doubled YAG 532 nm laser and 1200 gr per mm grating were used for this study, while the exposure time was set at 20 seconds and 5 scans were collected for each sample to improve the signal-to-noise ratio. Experiments were performed on the as-synthesized/as-received materials deposited on a glass slide in the range  $400\text{--}4000\text{ cm}^{-1}$ .

## 3. Results and discussion

### 3.1. Characterization of NIMs and ionized PEGs

ATR FT-IR spectroscopy was used to confirm the successful reaction between the primary amine of PEG and the sulfonate groups of the surface-modified nanoparticles. The ATR FT-IR spectra of PEG1K, Ionized PEG1K and NIM-PEG1K-E were shown in Fig. 2. Unlike that of PEG1K, the spectrum of Ionized

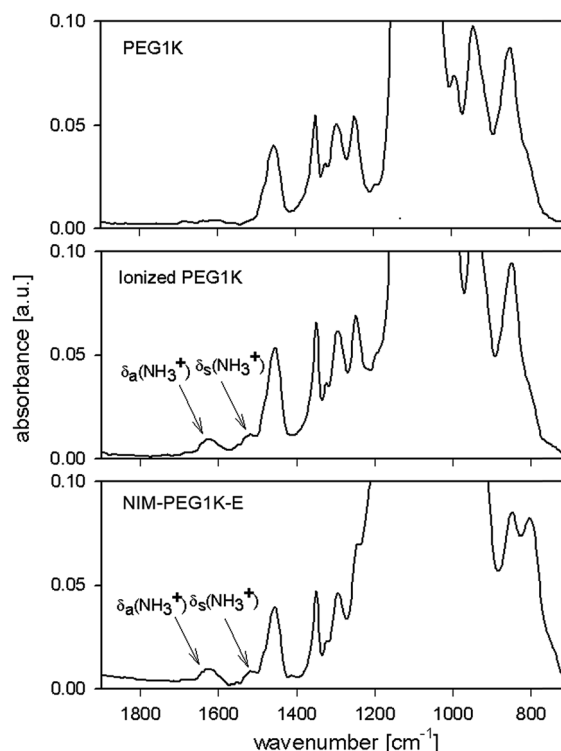


Fig. 2 ATR FT-IR spectra of PEG1K, Ionized PEG1K and NIM-PEG1K-E.

PEG1K exhibited bands related to the protonated amine vibration bands, *i.e.*,  $\delta_s(\text{NH}_3^+)$  symmetric bending mode) at  $1530\text{ cm}^{-1}$  and  $\delta_a(\text{NH}_3^+)$  asymmetric bending mode) at  $1630\text{ cm}^{-1}$ . These bands confirmed the acid-base reaction between the primary amine groups and the sulfonic groups. Water vibration band also appears at  $1630\text{ cm}^{-1}$  like protonated amines. However, the NIMs samples were dried prior to taking the FTIR spectra and this has been confirmed by thermogravimetric analyses. Therefore, the band is assigned to protonated amines. For NIM-PEG1K-E, the protonated amine bands were also observed, indicating that the same acid-base reaction occurred, and suggesting that PEG1K was successfully grafted onto the modified nanoparticles. The protonated amine bands were also seen in the other materials: NIM-PEG2K, NIM-PEG5K, Ionized PEG2K and Ionized PEG5K. It must be noted that sulfonate vibration bands cannot be used to confirm the reaction as the vibration region overlaps with that of other bonds ( $1100\text{--}1400\text{ cm}^{-1}$ ).

### 3.2. Roles of canopy and core on thermal stability

**Role of canopy on thermal stability.** Prior to investigating the role of the canopy on the thermal stability of NIMs, the thermal stability of unbound PEGs was tested and set as a baseline (Fig. S2 ESI†). The decomposition temperature  $T_{50}$  (as measured at the point of 50% mass loss) was used as an indicator to compare thermal stability of different materials.<sup>28</sup> The unbound PEGs, regardless of molecular weights, all started to degrade at around  $175\text{ }^\circ\text{C}$  (ref. 29) and their decomposition temperatures were all around  $200\text{ }^\circ\text{C}$ . Next, the unbound PEGs were ionized

with THOPS to form Ionized PEGs. The decomposition temperatures of Ionized PEGs all became much higher than those of the unbound PEGs: 98 °C higher in Ionized PEG1K, 63 °C higher in Ionized PEG2K and 25 °C higher in Ionized PEG5K. This enhancement could be due to the ionic bonding existing in Ionized PEGs that changed the chemistry of the system and therefore its decomposition pattern.<sup>30</sup> More precisely, the enhanced thermal stability of Ionized PEG could be due to the fact that THOPs modified the chemical reactions involved in the degradation of the polymer leading to more stable products and/or slower degradation kinetics.<sup>30</sup> Interestingly, the enhancement was most pronounced for Ionized PEG1K, suggesting that the contribution of a single ionic bond on thermal stability was higher for a shorter polymer chain. While the canopy size increased, the contribution from the single ionic bond on thermal stability to Ionized PEG was reduced.

Comparison between the thermal stabilities of NIMs and those of the unbound PEGs were shown in Fig. S3 and S4 (ESI†). NIMs exhibited even higher decomposition temperatures than those for the unbound PEGs: 123 °C higher in NIM-PEG1K, 100 °C higher in NIM-PEG2K, and 85 °C higher in NIM-PEG5K. NIMs were also more stable than the Ionized PEGs, although the enhancement was less pronounced than in the case of the pure PEGs. The only difference between Ionized PEGs and NIMs was the presence of inorganic nanoparticles (*i.e.*, silica nanoparticles). Thus the significant thermal stability enhancement of NIMs suggested that the presence of the nanoparticles also improved the thermal resistance. Similarly, the enhancement was also more pronounced in NIMs with shorter polymer chains.

Besides, a noteworthy feature can be found in Fig. S3 and S4:† during the mass change from 100% to 60%, NIM-PEG5K-E exhibited a linear decomposition curve while NIM-PEG1K-E and NIM-PEG2K-E exhibited non-linear decomposition curves. This indicated that the initial degradation of NIM-PEG5K-E was not delayed and it decomposed steadily after the initial degradation. This difference was possibly due to the fact that NIM-PEG5K-E had a large canopy size whose free ends of the polymer chains were relatively “far” from the surface of the nanoparticle. The thermal degradation of a polymeric chain usually starts from weak sites, such as an unstable end or side chain groups.<sup>30</sup> Therefore, the decomposition of the terminal groups of NIM-PEG5K-E was likely similar to that of untethered polymers. In contrast, the canopies in NIM-PEG1K-E and NIM-PEG2K-E were shorter and “closer” to the surface-modified nanoparticles.

**Role of the core in thermal stability.** While the exact mechanisms of the improved thermal stability of the polymer chains grafted onto inorganic substrates has been debated, there are a number of hypotheses. In polymer nanocomposites, the thermal stability enhancement was commonly thought to be caused by one or several of the following effects: (i) the so-called “barrier effect” in which the nanofillers formed a physical barrier limiting the diffusion of oxygen in the materials and that of the degradation products, (ii) the restrictive thermal motions caused by the presence of the nanoparticles that affect the transport of reactive species, (iii) the catalytic effect due to the

fact that the nanofillers modified the degradation reaction pathways, and (iv) the physical cross-linking or the adsorption of the polymer on the surface of the nanofillers.<sup>29,31–41</sup>

First, the potential contribution of (iv) was investigated. NIM-I-PEG1K-E, NIM-I-PEG2K-E and NIM-I-PEG5K-E were synthesized with a 1 : 1 ratio of sulfonate groups to amine groups. Thus, these NIMs contained the same number of moles of PEG but exhibited different core fractions (*i.e.*, lower the core fraction for longer polymer chains) and different degrees of surface contact between the polymer phase and the inorganic core phase. Therefore, NIM-I-PEG2K-25 and NIM-I-PEG5K-25, both with a 25 wt% core fraction, were synthesized to create the same degree of surface contact as NIM-I-PEG1K-E. As seen in Fig. S5 (ESI†), NIM-I-PEG1K-E still exhibited the highest thermal stability among the three NIMs, followed by NIM-I-PEG2K-25 and then NIM-I-PEG5K-25. This result ruled out the effect (iv) indicating that the surface contact between the nanoparticles and the polymer chains was not a dominant factor in enhancing the thermal stability of NIMs investigated in this study.

Next, a physical mixture of PEG and nanoparticles was prepared and labeled as PEG1K/NP-25. The main difference between this sample and NIM-I-PEG1K was the absence of a covalent bond between the alkoxy silane and the silica nanoparticles. Therefore, in PEG1K/NP-25, only physical and weak chemical interactions existed between PEG and the nanoparticles. Fig. 3 summarized and compared the thermal stabilities of PEG1K, PEG1K/NP-25, Ionized PEG1K, and NIM-I-PEG1K. PEG1K/NP-25 exhibited no enhancement in thermal stability compared to PEG1K, despite physical and weak chemical interactions between PEG and the nanoparticles indicating that the addition of silica nanoparticles did not cause any positive contribution to the thermal stability. A similar observation was also reported by Lu and Huang for a mixture of silica nanoparticles and polymaleimide.<sup>42</sup> This result suggested that the enhancement of the thermal stability in NIMs was not related to the barrier effect (i), since this effect should be

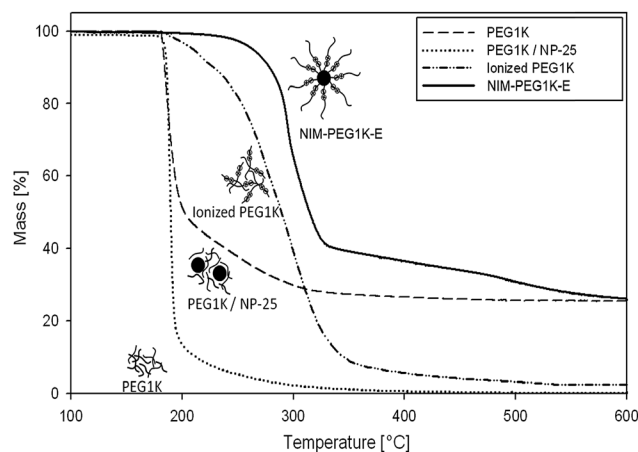


Fig. 3 Thermal stability of PEG1K, PEG1K/NP-25, Ionized PEG1K and NIM-PEG1K-E in oxygen environment with a ramping rate 5 °C min<sup>-1</sup>.



independent of the types of interaction and bonding between the polymer chains and the core.

In summary, as illustrated in Fig. 3 the most dominant factor leading to the enhancement of thermal stability of the studied hybrid materials was the strong chemical interactions between the polymer chains and the functionalized nanoparticles or even among polymer chains: the presence of silane, the ionic bond between the alkoxy silane and PEG, and the covalent bond between the ionized polymer and the silica nanoparticles. As discussed earlier, in NIMs, the polymer chains would have fewer weak sites (*i.e.*, sites where polymer degradation is usually initiated) than the unbound polymer as one side of the polymer in NIMs was grafted onto the inorganic core. This may have modified the degradation reaction pathways of tethered polymers. An additional reason, that does not exclude the previous one, could be that tethering one end of the polymer onto the core further limited the thermal motions of the polymer compared to the unbound polymer, and therefore, slowed down the transport of the reactive species (the effect (iii)).

**Long-term thermal stability.** Tuning the canopy size and introducing the additional bonding remarkably enhanced the thermal stability of NIMs, which is extremely important for adsorption applications at elevated temperatures. The higher decomposition temperature ensured a wider operational temperature range which is critical to applications of gas absorption like CO<sub>2</sub> capture. In CO<sub>2</sub> capture, liquid materials have been shown to require elevated temperatures (*e.g.*, 120 °C) for regeneration over multiple cycles. Therefore, long-term thermal stability of NIMs has been shown to be a crucial aspect of the carbon capture process. CO<sub>2</sub> capture materials (*e.g.*, amine solvents) are regenerated typically at 120 °C (*ref.* 43) to break the carbamate bond formed upon reaction between CO<sub>2</sub> and amine groups. Herein, the thermal stability of NIM-PEG1K was tested during a series of temperature swing cycles at 120 °C. The results were compared to those for untethered polymer, PEG1K. The mass loss of NIM-PEG1K and PEG1K as a function of the number of temperature swing cycles

(between 20 °C and 120 °C) was represented in Fig. 4. While the mass loss of PEG1K was about 80% after the 100 cycles, that of NIM-PEG1K was less than 5%. At a higher temperature (140 °C), the greater long-term thermal stability of NIMs compared to PEG1K was also observed. Consequently the enhanced thermal stability of NIMs described above significantly increased their long-term thermal stability.

### 3.3. Thermally-induced swelling

Despite the fact that polymer chains of the canopy were tethered to the corona, they could still adopt different conformations in response to environmental stimuli. The temperature was one of these environmental changes that could affect the conformation of the polymer chains, subsequently leading to a volume change of the materials. The effect of the canopy size (*i.e.*, the polymer chain length) on the thermally-induced swelling of NIMs was examined. The thermally-induced swelling of NIMs and their corresponding PEGs with various canopy sizes obtained in the temperature range from 60 °C to 120 °C (*i.e.*, typical CO<sub>2</sub> capture and regeneration temperatures, respectively) were represented in Fig. 5. As described in eqn (1), the swelling percentage was calculated by comparing the absorbance of the CH<sub>2</sub> stretching band in NIMs at given temperatures (70–120 °C) and at 60 °C. As seen in Fig. 5, an increase in temperature caused a noticeable swelling in both NIMs and PEGs ranging from 7% to 12%. In the case of unbound PEG, the effect of the polymer chain length was negligible and all three PEGs exhibited around 2% swelling every 10 degree increase in temperature. Interestingly, NIMs consistently exhibited smaller thermally-induced swelling of the polymer chains than their corresponding PEGs. Considering that the rigidity of silica nanocores and therefore their negligible contribution to volume change during a thermal or pressure swing, this difference could be attributed to the restriction of the motion of the polymer chains in NIMs' canopy. While the effect of the canopy size on the thermal stability of PEGs was negligible, it was pronounced in the case of NIMs. For a given increase in

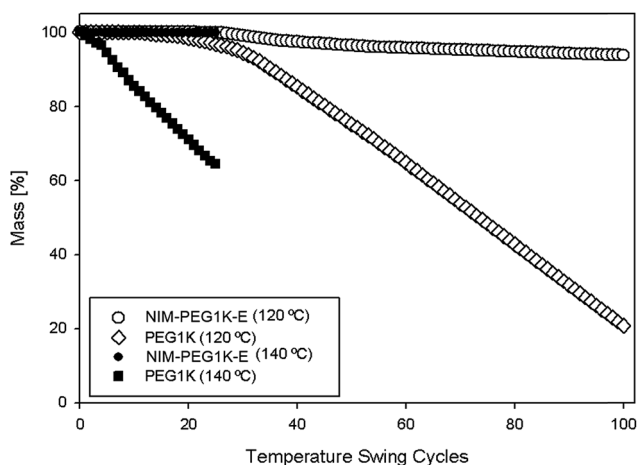


Fig. 4 Cyclic thermal stability of NIM-PEG1K-E and PEG1K (temperature swing from 20 °C to 120 °C/140 °C with a ramping rate 5 °C min<sup>-1</sup> and isothermal for 5 minutes, each cycle is 25/29 minutes).

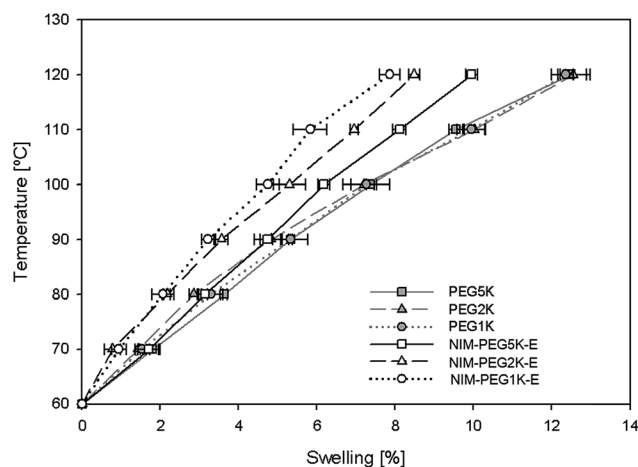


Fig. 5 Thermally-induced swelling of NIMs with various chain lengths (conducted at  $P_{\text{CO}_2} = 0$  MPa).

temperature, NIM-PEG5K exhibited the highest swelling, followed by NIM-PEG2K and then NIM-PEG1K, suggesting a smaller thermally-induced swelling for NIMs with shorter chain lengths. This trend could be due to the fact that NIM-PEG5K had a higher polymer fraction (95 wt%), resulting in its behavior being closer to that of untethered polymers.

### 3.4. CO<sub>2</sub> capture capacity and CO<sub>2</sub>-induced swelling

The presence of CO<sub>2</sub> in the vapor phase or physically absorbed in NIMs could potentially induce conformational changes of the polymeric canopy, and cause swelling. This aspect was investigated according to the reported procedure based on ATR FT-IR spectroscopy.<sup>16,26,27</sup>

Compared to NIMs, the unbound PEGs used in the synthesis of NIMs contained a terminal primary amine group. This functional group could interact with CO<sub>2</sub> chemically and therefore interfere with the CO<sub>2</sub>-induced swelling behavior arising from CO<sub>2</sub> physisorption. Hence, methoxy-polyethylene glycols (*i.e.*, mPEG1K, 2K and 5K), which were deprived of any amine group, were used for this particular study to substitute the original unbound amine-terminated PEGs.

**CO<sub>2</sub> capture capacity.** CO<sub>2</sub> capture capacities of NIMs and their corresponding mPEGs were shown in Fig. S6 (ESI†). The silica nanoparticles used in the synthesis of NIMs were nonporous and thus the silica nanoparticles were not considered as active components for CO<sub>2</sub> absorption. Therefore, the capacity of NIMs shown here was solely based on their organic component, which was referred in Fig. S6† as “solvents”. As seen in Fig. S6,† CO<sub>2</sub> capture capacities of mPEG did not vary significantly with the canopy size. This was because CO<sub>2</sub> solubility was mostly affected by the total amount of ether groups in the solvent, forming Lewis acid–base interactions with CO<sub>2</sub>.<sup>14,44,45</sup> Since the CO<sub>2</sub> absorption capacity was normalized for

a given mass of mPEGs, similar total amounts of ether groups were present regardless the length of the polymer. The CO<sub>2</sub> capture capacities of NIMs were slightly lower than those of mPEGs but the difference was not significant. NIMs with shorter chains resulted in slightly lower CO<sub>2</sub> capture capacity. The reason for such differences may be attributed to the presence of the linker materials, alkoxyisilane (THOPS), in NIMs. Since THOPS did not contain functional groups able to chemically react with CO<sub>2</sub>, the presence of THOPS increased the total organic portion of NIMs but did not contribute to CO<sub>2</sub> absorption. Therefore, NIMs exhibited lower CO<sub>2</sub> capture capacities than mPEGs. The existence of the alkoxyisilane had the most notable effect on the CO<sub>2</sub> absorption capacity of NIMs with the smallest canopy (*i.e.*, NIM-PEG1K-E) whose weight fraction of THOPS against PEG was the highest.

**CO<sub>2</sub>-induced swelling.** In addition to thermally-induced swelling, NIMs could also experience a volume change in response to the absorption of gas molecules such as CO<sub>2</sub>.<sup>16,17,19</sup> In order to correlate the actual amounts of CO<sub>2</sub> loaded in the materials and their swelling behaviors, the CO<sub>2</sub> capture capacities of NIMs and mPEGs were measured and were reported as a function of the CO<sub>2</sub>-induced swelling in Fig. 6(a). As discussed earlier, the canopy size did not affect significantly the thermally-induced swelling behavior and CO<sub>2</sub> absorption capacity. Therefore, mPEGs exhibited similar CO<sub>2</sub>-induced swelling behaviors regardless the canopy size. The largest swelling measured for mPEGs was about 21% at the highest measured absorption capacity.

Once PEGs were grafted onto the nanoparticles, swelling was less pronounced (15–19%) for the same CO<sub>2</sub> absorption capacity level. The reduced swelling of NIMs compared to untethered PEGs was observed in prior studies as well.<sup>16,19</sup> It was assigned to the conformational difference between NIMs and unbound polymers. As polymer chains were grafted onto nanoparticles,

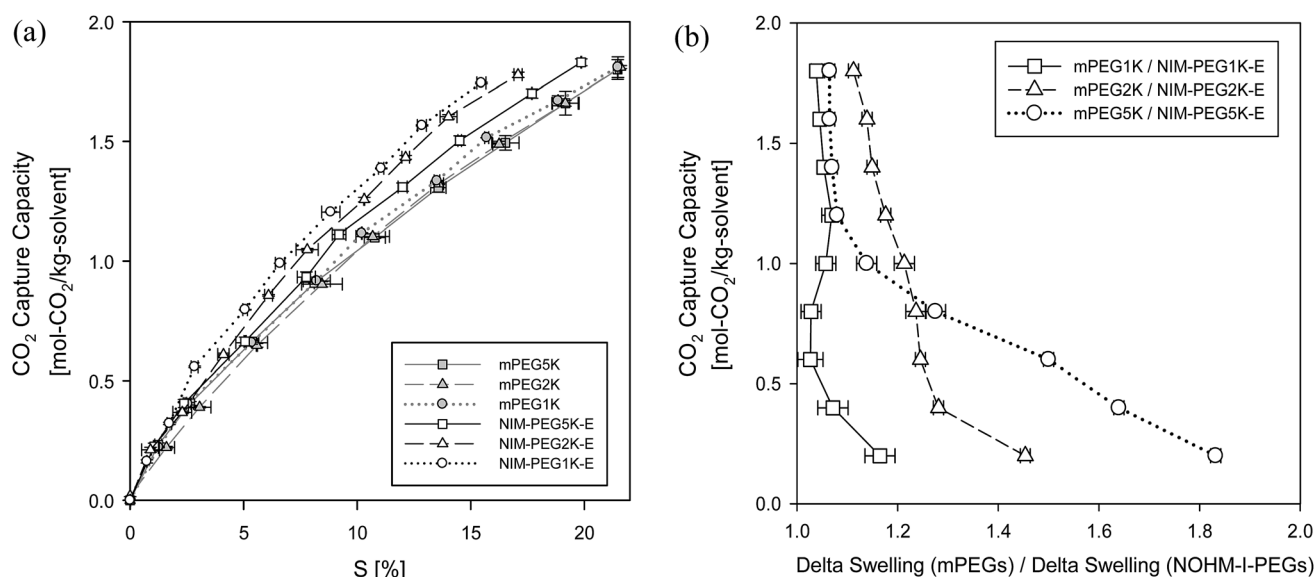


Fig. 6 Effect of chain length on: (a) CO<sub>2</sub>-induced swelling of mPEG and NIM-PEGs and (b) the ratio of delta swelling of mPEG to NIM-PEGs at 60 °C and  $P_{\text{CO}_2} = 0.40\text{--}5.57$  MPa. The amount of swelling percentage caused by 0.2 mmol g<sup>-1</sup> CO<sub>2</sub> capture capacity was defined as a delta swelling.

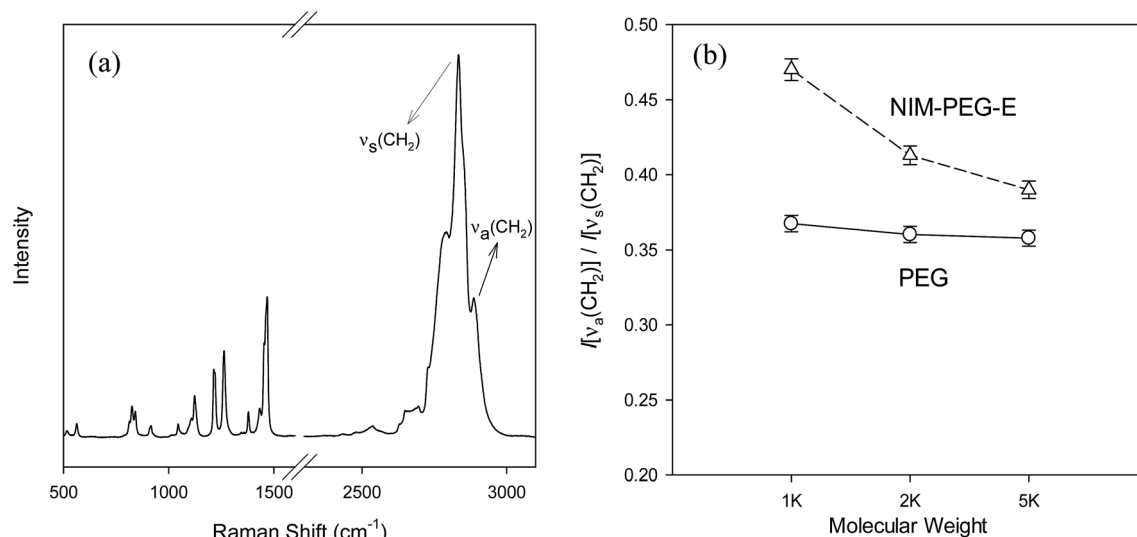


Fig. 7 Results of the conformational study with: (a) the Raman spectrum of PEG1K in the range from 400 to 3100 cm<sup>-1</sup> and (b) the ratios of Raman spectral intensity of ν<sub>a</sub>(CH<sub>2</sub>) to ν<sub>s</sub>(CH<sub>2</sub>) for PEGs and NIM-PEG samples with different molecular weights.

they adopted a frustrated structure in which they tended to stretch out to fill the space between the nanoparticles.<sup>16,19</sup> Therefore, a greater ordering of the polymer chains was observed in NIMs compared to the unbound PEGs, as shown in prior studies.<sup>16,19</sup> The structural frustration undergone by the polymer chains in NIMs led to an entropy change that favored the absorption of CO<sub>2</sub> with relatively smaller volume increase compared to the unbound polymers.<sup>16,19</sup> As shown in Fig. 6(a), NIMs with smaller canopy sizes swelled less for a given CO<sub>2</sub> capture capacity. This suggests that the conformational ordering in NIMs was more pronounced for shorter canopy, *i.e.* lower organic content. Another interesting feature found in Fig. 6(a) was that for each mPEG, a steady increase in its swelling was observed at regular intervals of CO<sub>2</sub> absorbed (*e.g.*, 0.2 mmol g<sup>-1</sup>), whereas this was not the case for NIMs.

In order to further investigate the swelling behaviors of NIMs and their corresponding polymers, the rate of swelling at each CO<sub>2</sub> absorption capacity was calculated and was referred to as “delta swelling”. The ratios of the delta swelling of the polymer to that of the corresponding NIMs (normalized swelling behavior) were plotted against the CO<sub>2</sub> absorption capacity in Fig. 6(b). Fig. 6(b) displayed the effect of the canopy size on the deviation of CO<sub>2</sub>-induced swelling behaviors between mPEG and NIMs. With the smallest chain length in this study, mPEG1K and NIM-PEG1K-E showed the most distinct swelling behaviors with a ratio of 1.8 at the low CO<sub>2</sub> capture capacity. On the other hand, mPEG5K and NIM-PEG5K exhibited a ratio close to 1 regardless the level of CO<sub>2</sub> absorption capacity, indicating similar CO<sub>2</sub>-induced swelling behaviors. Interestingly, at higher CO<sub>2</sub> absorption capacities, the ratios of delta swellings all approached 1, revealing that the structural effect on the swelling behaviors of NIMs was most dominant during the initial CO<sub>2</sub> absorption in the materials. In other words, the conformational structure of polymer chains in NIMs initially allowed more CO<sub>2</sub> to be

absorbed in NIMs with the same volume change as mPEG. Then, as the conformational difference between NIMs and mPEG progressively vanished due to the continued absorption of CO<sub>2</sub>, NIMs started to behave similarly to mPEG in terms of CO<sub>2</sub>-induced swelling behaviors.

To further verify the relationship between conformational order in NIMs and their swelling behaviors, Raman spectroscopy, which was proposed to determine the conformational order of linear molecules, was employed.<sup>46,47</sup> Indeed, the Raman spectra of polymers provided specific indicators that could be used to characterize the conformational change of linear molecules. Fig. 7(a) showed a typical Raman spectrum of PEG (PEG1K). Since CH<sub>2</sub> group was the backbone unit of PEG, the intensity (*I*) ratio of ν<sub>a</sub>(CH<sub>2</sub>) band (asymmetric stretching mode, ~2850 cm<sup>-1</sup>) to ν<sub>s</sub>(CH<sub>2</sub>) band (symmetric stretching mode, ~2885 cm<sup>-1</sup>) was used as an indicator of conformational order in large molecules.<sup>47</sup> The spectra of PEG and NIMs in the ν<sub>a</sub>(CH<sub>2</sub>) and ν<sub>s</sub>(CH<sub>2</sub>) regions were obtained before their exposure to CO<sub>2</sub> and were shown in Fig. S7 (ESI<sup>†</sup>). The ratios of  $I[\nu_a(\text{CH}_2)]$  to  $I[\nu_s(\text{CH}_2)]$  of each spectrum were then calculated and plotted in Fig. 7(b). The ratios of  $I[\nu_a(\text{CH}_2)]$  to  $I[\nu_s(\text{CH}_2)]$  of PEGs were comparable to each other, indicating that the effect of canopy size on the conformational order in the case of unbound polymers was negligible. However, once PEG was grafted onto the surface-functionalized nanoparticles to form NIMs, the ratio of  $I[\nu_a(\text{CH}_2)]$  to  $I[\nu_s(\text{CH}_2)]$  of each NIM-PEG was notably higher than that of its corresponding PEG. This implied that the structural modification in NIMs was successful and the polymer chains of NIMs had a greater conformational order than that of the unbound PEG. NIM-PEG1K-E exhibited the highest increase in terms of intensity ratio among the three NIMs samples, followed by NIM-PEG2K-E and NIM-PEG5K-E. This further supported the hypothesis given for the trend found in swelling behaviors as a function of conformational orders.



## 4. Conclusions

In this study, the structure–property relationships of NIMs were investigated. Particularly, the roles of the canopy and core on the thermal stability, swelling behaviors and CO<sub>2</sub> capture capacity of NIMs were studied. Compared to the unbound polymers as well as a physical mixture of polymers and nanoparticles, NIMs exhibited enhanced thermal stability (up to 100 °C enhancement). This enhancement was predominantly attributed to: (i) the presence of the silane, (ii) the ionic bond between the corona and polymeric canopy, and (iii) the covalent bond between the silane and the silica nanoparticles. These three features must have modified the chemical reaction pathways of the polymer degradation, reduced the number of weak sites, and caused restrictive thermal motions, all explaining the enhanced thermal stability. In contrast, the physical adsorption of the polymer chains onto the surface of the nanoparticles and the so-called barrier effect were found to less likely affect the thermal stability of the studied materials. The thermal stability enhancement allowed NIMs to sustain up to at least 100 temperature swing cycles at 120 °C with minimal weight loss. On the other hand, the corresponding unbound polymers experienced a 80% mass loss within the same number of thermal cycles. The swelling studies of NIMs indicated that grafting of polymer chains onto the cores resulted in a more ordered structure of polymer chains in NIMs compared to the unbound polymer, and this in turn led to 10–30% less swelling in NIMs during both thermal cycle and CO<sub>2</sub> sorption (*i.e.*, 15–19% for NIMs *vs.* 21% for PEG). This study on the effect of canopy size on thermal stability and swelling behaviors of the materials provided valuable information to optimize NIMs for future applications including CO<sub>2</sub> capture.

## Acknowledgements

This publication was based on work supported by Award no. KUS-C1-018-02, made by King Abdullah University of Science and Technology (KAUST).

## References

- 1 Z.-M. Huang, Y. Z. Zhang, M. Kotaki and S. Ramakrishna, A review on polymer nanofibers by electrospinning and their applications in nanocomposites, *Compos. Sci. Technol.*, 2003, **63**, 2223–2253.
- 2 J. Jordan, K. I. Jacob, R. Tannenbaum, M. A. Sharaf and I. Jasiuk, Experimental trends in polymer nanocomposites—a review, *Mater. Sci. Eng., A*, 2005, **393**, 1–11.
- 3 S. Sinha Ray and M. Okamoto, Polymer/layered silicate nanocomposites: a review from preparation to processing, *Prog. Polym. Sci.*, 2003, **28**, 1539–1641.
- 4 A. C. Balazs, T. Emrick and T. P. Russell, Nanoparticle Polymer Composites: Where Two Small Worlds Meet, *Science*, 2006, **314**, 1107–1110.
- 5 R. Shenhar, T. B. Norsten and V. M. Rotello, Polymer-Mediated Nanoparticle Assembly: Structural Control and Applications, *Adv. Mater.*, 2005, **17**, 657–669.
- 6 D. S. Ginger, H. Zhang and C. A. Mirkin, The Evolution of Dip-Pen Nanolithography, *Angew. Chem., Int. Ed.*, 2004, **43**, 30–45.
- 7 C. M. Niemeyer, Nanoparticles, Proteins, and Nucleic Acids: Biotechnology Meets Materials Science, *Angew. Chem., Int. Ed.*, 2001, **40**, 4128–4158.
- 8 M. P. Pileni, Nanocrystal Self-Assemblies: Fabrication and Collective Properties, *J. Phys. Chem. B*, 2001, **105**, 3358–3371.
- 9 A. L. Rogach, D. V. Talapin, E. V. Shevchenko, A. Kornowski, M. Haase and H. Weller, Organization of Matter on Different Size Scales: Monodisperse Nanocrystals and Their Superstructures, *Adv. Funct. Mater.*, 2002, **12**, 653–664.
- 10 E. C. Scher, L. Manna and A. P. Alivisatos, Shape control and applications of nanocrystals, *Philos. Trans. R. Soc., A*, 2003, **361**, 241–257.
- 11 V. Tohver, A. Chan, O. Sakurada and J. A. Lewis, Nanoparticle Engineering of Complex Fluid Behavior, *Langmuir*, 2001, **17**, 8414–8421.
- 12 A. B. Bourlinos, S. R. Chowdhury, R. Herrera, N. Chalkias, D. D. Jiang, Q. Zhang, L. A. Archer and E. P. Giannelis, Functionalized Nanostructures with Liquid-Like Behavior: Expanding the Gallery of Available Nanostructures, *Adv. Funct. Mater.*, 2005, **15**, 1285–1290.
- 13 A. B. Bourlinos, R. Herrera, N. Chalkias, D. D. Jiang, Q. Zhang, L. A. Archer and E. P. Giannelis, Surface-Functionalized Nanoparticles with Liquid-Like Behavior, *Adv. Mater.*, 2005, **17**, 234–237.
- 14 K.-Y. A. Lin and A.-H. A. Park, *Effects of Bonding Types and Functional Groups on CO<sub>2</sub> Capture using Novel Multiphase Systems of Liquid-like Nanoparticle Organic Hybrid Materials Environmental Science & Technology*, 2011.
- 15 K.-Y. A. Lin, C. Petit and A.-H. A. Park, Effect of SO<sub>2</sub> on CO<sub>2</sub> Capture Using Liquid-like Nanoparticle Organic Hybrid Materials, *Energy Fuels*, 2013, **27**, 4167–4174.
- 16 Y. Park, J. Decatur, K.-Y. A. Lin and A.-H. A. Park, Investigation of CO<sub>2</sub> Capture Mechanisms of Liquid-like Nanoparticle Organic Hybrid Materials via Structural Characterization, *Phys. Chem. Chem. Phys.*, 2011, **13**, 18115–18122, DOI: 10.1039/c1cp22631b.
- 17 Y. Park, D. Shin, Y. N. Jang and A.-H. A. Park, CO<sub>2</sub> Capture Capacity and Swelling Measurements of Liquid-like Nanoparticle Organic Hybrid Materials via Attenuated Total Reflectance Fourier Transform Infrared Spectroscopy, *J. Chem. Eng. Data*, 2011, **57**, 40–45.
- 18 C. Petit, K.-Y. A. Lin and A.-H. A. Park, Design and Characterization of Liquid-like POSS-based Hybrid Nanomaterials Synthesized via Ionic Bonding and Their Interactions with CO<sub>2</sub>, *Langmuir*, 2013, **29**, 12234–12242.
- 19 C. Petit, Y. Park, K.-Y. A. Lin and A.-H. A. Park, Spectroscopic Investigation of the Canopy Configurations in Nanoparticle Organic Hybrid Materials of Various Grafting Densities during CO<sub>2</sub> Capture, *J. Phys. Chem. C*, 2011, **116**, 516–525.
- 20 R. Rodriguez, R. Herrera, L. A. Archer and E. P. Giannelis, Nanoscale Ionic Materials, *Adv. Mater.*, 2008, **20**, 4353–4358.

- 21 N. J. Fernandes, T. J. Wallin, R. A. Vaia, H. Koerner and E. P. Giannelis, Nanoscale Ionic Materials, *Chem. Mater.*, 2013, **26**, 84–96.
- 22 B. Hong and A. Z. Panagiotopoulos, Molecular Dynamics Simulations of Silica Nanoparticles Grafted with Poly(ethylene oxide) Oligomer Chains, *J. Phys. Chem. B*, 2012, **116**, 2385–2395.
- 23 N. Fernandes, P. Dallas, R. Rodriguez, A. B. Bourlinos, V. Georgakilas and E. P. Giannelis, Fullerol ionic fluids, *Nanoscale*, 2010, **2**, 1653–1656.
- 24 L. Wu, B. Zhang, H. Lu and C.-Y. Liu, Nanoscale ionic materials based on hydroxyl-functionalized graphene, *J. Mater. Chem. A*, 2014, **2**, 1409–1417.
- 25 M. L. Jespersen, P. A. Mirau, E. D. von Meerwall, H. Koerner, R. A. Vaia, N. J. Fernandes and E. P. Giannelis, Hierarchical Canopy Dynamics of Electrolyte-Doped Nanoscale Ionic Materials, *Macromolecules*, 2013, **46**, 9669–9675.
- 26 N. M. B. Flichy, S. G. Kazarian, C. J. Lawrence and B. J. Briscoe, An ATR-IR Study of Poly(Dimethylsiloxane) under High-Pressure Carbon Dioxide: Simultaneous Measurement of Sorption and Swelling, *J. Phys. Chem. B*, 2001, **106**, 754–759.
- 27 I. Pasquali, J.-M. Andanson, S. G. Kazarian and R. Bettini, Measurement of CO<sub>2</sub> sorption and PEG 1500 swelling by ATR-IR spectroscopy, *J. Supercrit. Fluids*, 2008, **45**, 384–390.
- 28 N. Wang, Q. Fang, E. Chen, J. Zhang and Y. Shao, Structure, crystallization behavior, and thermal stability of PP/MCM-41 nanocomposite, *Polymer Eng. Sci.*, 2009, **49**, 2459–2466.
- 29 J. W. Gilman, Flammability and thermal stability studies of polymer layered-silicate (clay) nanocomposites, *Appl. Clay Sci.*, 1999, **15**, 31–49.
- 30 V. Mittal, Thermal Characterization of Fillers and Polymer Nanocomposites, in *Characterization Techniques for Polymer Nanocomposites*, Wiley-VCH Verlag GmbH & Co. KGaA, 2012, pp. 13–32.
- 31 P. Liu and Z. Su, Thermal stabilities of polystyrene/silica hybrid nanocomposites via microwave-assisted in situ polymerization, *Mater. Chem. Phys.*, 2005, **94**, 412–416.
- 32 H. Sugimoto, K. Daimatsu, E. Nakanishi, Y. Ogasawara, T. Yasumura and K. Inomata, Preparation and properties of poly(methylmethacrylate)–silica hybrid materials incorporating reactive silica nanoparticles, *Polymer*, 2006, **47**, 3754–3759.
- 33 J. W. Gilman, C. L. Jackson, A. B. Morgan, R. Harris, E. Manias, E. P. Giannelis, M. Wuthenow, D. Hilton and S. H. Phillips, Flammability Properties of Polymer-Layered-Silicate Nanocomposites. Polypropylene and Polystyrene Nanocomposites, *Chem. Mater.*, 2000, **12**, 1866–1873.
- 34 Z. Peng and L. X. Kong, A thermal degradation mechanism of polyvinyl alcohol/silica nanocomposites, *Polym. Degrad. Stab.*, 2007, **92**, 1061–1071.
- 35 Z. Peng, L. X. Kong and S.-D. Li, Thermal properties and morphology of a poly(vinyl alcohol)/silica nanocomposite prepared with a self-assembled monolayer technique, *J. Appl. Polym. Sci.*, 2005, **96**, 1436–1442.
- 36 D. M. Marquis, E. Guillaume and C. Chivas-Joly, *Nanocomposites and Polymers with Analytical Methods*, Intech, 2011.
- 37 E. P. Giannelis, Polymer Layered Silicate Nanocomposites, *Adv. Mater.*, 1996, **8**, 29–35.
- 38 S. Pavlidou and C. D. Papaspyrides, A review on polymer-layered silicate nanocomposites, *Prog. Polym. Sci.*, 2008, **33**, 1119–1198.
- 39 L. A. Utracki, *Clay-Containing Polymeric Nanocomposites*, Rapra, Shawbury, 2004.
- 40 M. Zanetti, P. Bracco and L. Costa, Thermal degradation behaviour of PE/clay nanocomposites, *Polym. Degrad. Stab.*, 2004, **85**, 657–665.
- 41 J. Zhu, A. B. Morgan, F. J. Lamelas and C. A. Wilkie, Fire Properties of Polystyrene–Clay Nanocomposites, *Chem. Mater.*, 2001, **13**, 3774–3780.
- 42 G. T. Lu and Y. Huang, Synthesis of polymaleimide/silica nanocomposites, *J. Mater. Sci.*, 2002, **37**, 2305–2309.
- 43 G. S. Goff and G. T. Rochelle, Monoethanolamine Degradation: O<sub>2</sub> Mass Transfer Effects under CO<sub>2</sub> Capture Conditions, *Ind. Eng. Chem. Res.*, 2004, **43**, 6400–6408.
- 44 S. G. Kazarian, M. F. Vincent, F. V. Bright, C. L. Liotta and C. A. Eckert, Specific Intermolecular Interaction of Carbon Dioxide with Polymers, *J. Am. Chem. Soc.*, 1996, **118**, 1729–1736.
- 45 H. Lin and B. D. Freeman, Gas solubility, diffusivity and permeability in poly(ethylene oxide), *J. Membr. Sci.*, 2004, **239**, 105–117.
- 46 K. Larsson and R. P. Rand, Detection of changes in the environment of hydrocarbon chains by Raman spectroscopy and its application to lipid-protein systems, *Biochim. Biophys. Acta, Lipids Lipid Metab.*, 1973, **326**, 245–255.
- 47 C. J. Orendorff, M. W. Ducey and J. E. Pemberton, Quantitative Correlation of Raman Spectral Indicators in Determining Conformational Order in Alkyl Chains, *J. Phys. Chem. A*, 2002, **106**, 6991–6998.